ACS APPLIED MATERIALS & INTERFACES

Research Article

www.acsami.org

Effects of Polymer Structure on Properties of Sulfonated Polyimide/Protic Ionic Liquid Composite Membranes for Nonhumidified Fuel Cell Applications

Tomohiro Yasuda, Shin-ichiro Nakamura, Yoshiyuki Honda, Kei Kinugawa, Seung-Yul Lee, and Masayoshi Watanabe*

Department of Chemistry and Biotechnology, Yokohama National University, 79-5 Tokiwadai, Hodogaya-ku, Yokohama 240-8501, Japan

Supporting Information

ABSTRACT: To investigate the effects of polymer structure on the properties of composite membranes including a protic ionic liquid, [dema][TfO] (diethylmethylammonium trifluoromethanesulfonate), for nonhumidified fuel cell applications, we synthesized sulfonated polyimides (SPIs) with different structures as matrix polymers, which have different magnitudes of ion-exchange capacities (IECs), different sequence distributions of ionic groups, and positions of sulfonate groups in the main chain or side chain. Despite having similar IECs, multiblock copolymer SPI and random copolymer SPI having sulfonate groups in the side chain exhibit higher ionic conductivity than random copolymer SPI having sulfonate groups in the main chain, indicating that the flexibility of sulfonic acid groups and the sequence distribution of ionic groups greatly affect the ion conduction. Atomic force microscopy observation revealed that the multiblock copolymer SPI forms more developed phase separation than the others. These results indicate that the flexibility of sulfonic acid groups and the connectivity of the ion conduction channel, which greatly depends on the sequence distribution, affect the ion conduction.

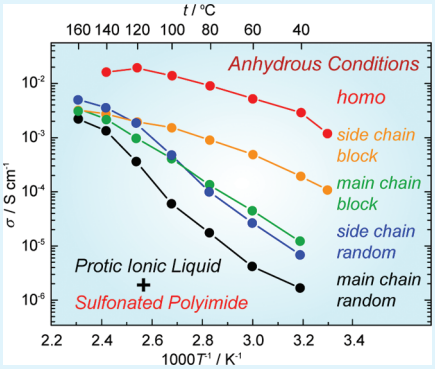

KEYWORDS: *protic ionic liquid, sulfonated polyimide, composite membrane, nonhumidifying fuel cell, ionic conductivity, morphology*

INTRODUCTION

Room temperature ionic liquids (RTILs) have drawn considerable attention as possible electrolytes for electrochemical devices such as lithium secondary batteries,[1−3] electric double layer capacitors,[4,5] actuators,[6,7] dye-sensitized solar cells,[8−11] and fuel cells[12−15] because they exhibit unique properties,[16] including negligible vapor pressure, excellent thermal stability, high ionic conductivity, and a wide potential window. To employ RTILs in such devices, it is preferable that the RTILs are solidified into mechanically tough membranes without disrupting their unique properties; such solidification enhances the performance, safety, long-term stability, and reliability of the devices and hence is a popular research topic.[17−19] However, the solidification of RTILs using matrix polymers frequently results in a trade-off relationship between the desirable RTIL properties and mechanical strength of the membranes. Suitable fabrication methods are under investigation by many researchers but have not yet been established.

Fuel cells that can be operated at intermediate temperatures (100−200 °C) under nonhumidified conditions[20−23] are of great importance because such systems offer the following advantages: (1) Water management systems are not necessary. (2) Control of cell temperature using a radiator becomes easy. (3) Poisoning of the Pt catalyst by CO can be suppressed. (4) Activity of the Pt catalyst toward fuel cell reactions is enhanced. We reported that certain protic RTILs prepared by neutralization of Brønsted acids and Brønsted bases can conduct protons and are active in fuel cell electrode reactions, i.e., hydrogen oxidation reactions and oxygen reduction reactions, under anhydrous conditions. Such protic RTILs can be employed as proton carriers in fuel cells under nonhumidified conditions.[12] We subsequently reported that diethylmethylammonium trifluoromethanesulfonate ([dema][TfO]) combines favorable bulk properties and interfacial electrochemical properties.[24] [dema][TfO] has a liquid phase with a wide temperature range (melting point (T_m) = −6 °C and decomposition temperature (T_d) = 360 °C), as well as a high ionic conductivity (σ = 55 mS cm^{-1} at 150 °C under anhydrous conditions). Additionally, fuel cell electrode reactions can proceed with a low overpotential in [dema][TfO]. The open circuit potential of a simple H_2/O_2 fuel cell using [dema][TfO], Pt electrodes, and a glass U-tube at 150 °C without humidification has been shown to be 1.03 V, which is close to the theoretical value at 150 °C. We also recently found that sulfonated polyimides (SPIs) in ammonium exhibit good compatibility with [dema][TfO].[25] Further, fuel cells have been

Received: January 6, 2012
Accepted: February 21, 2012
Published: February 21, 2012

(a) Protic ionic liquid

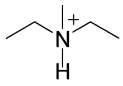

$CF_3SO_3^-$

diethylmethylammonium trifluoromethanesulfonate [dema][TfO]

(b) Matrix polymers

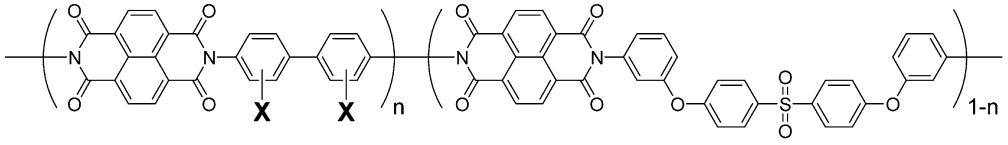

		position	X	n
***mr*-SPI**	main chain/random	**2,2'**	$-SO_3^-NHEt_2Me^+$	0.5, 0.8
***sr*-SPI**	side chain/random	**3,3'**	$-O(CH_2)_3SO_3^-NHEt_2Me^+$	0.5, 0.8
***homo*-SPI**	homopolymer	**2,2'**	$-SO_3^-NHEt_2Me^+$	1

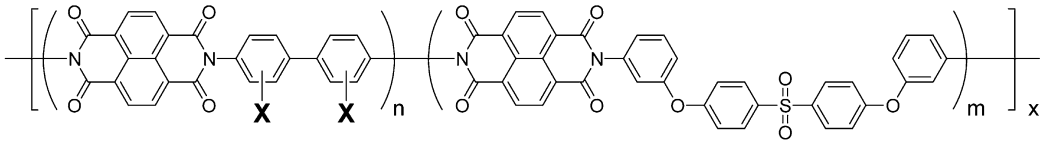

				n
***mb*-SPI**	main chain/block	**2,2'**	$-SO_3^-NHEt_2Me^+$	0.5
***sb*-SPI**	side chain/block	**3,3'**	$-O(CH_2)_3SO_3^-NHEt_2Me^+$	0.5

Figure 1. Chemical structures of [dema][TfO] and SPIs.

successfully operated under nonhumidified conditions using composite membranes.[26]

SPIs in proton form have been investigated by many researchers as proton-conducting polymer electrolyte membranes for conventional humidified polymer electrolyte fuel cells (PEFCs).[27−30] The objectives of these studies have commonly been the improvement of hydrolytic stability and proton conductivity (especially, at low relative humidity), which ensures high performance of the PEFCs using these membranes. However, there have been no investigations of the effects of the chemical structure of SPIs on the properties of RTIL/SPI composite membranes. In this study, we prepared structurally different SPIs, i.e., multiblock copolymers and random copolymers, SPIs with sulfo-groups in their main chains and side chains, and SPIs with different ion-exchange capacities (IECs). The properties of the corresponding composite membranes including [dema][TfO] were explored in correlation with their morphology and number of [dema]-[TfO] per sulfo groups.

EXPERIMENTAL SECTION

Materials. 1,4,5,8-Naphthalene tetracarboxylic dianhydride (NTDA) (90%, Aldrich) was soaked in DMF while stirring at 60 °C for 12 h. After filtration, NTDA was washed with acetone and dried under vacuum. 2,2′-Benzidinesulfonic acid (BDSA) (70%, Tokyo Kasei) and bis[4-(3-aminophenoxy)-phenyl]sulfone (3BAPPS) (95%, Wako Chem.) were purified according to a previously reported procedure.[26] 3,3′-Bis(sulfopropoxy)benzidine (BSPB) was synthesized as described in a previous report.[31] NTDA, BDSA, 3,3′-BSPB, and 3BAPPS were dried in a vacuum oven at 80 °C prior to use. *m*-Cresol (98%, Wako Chem.) was dried over 4A molecular sieves (Wako Chem.) prior to use. *N*,*N*-Diethylmethylamine (DEMA) (97%, Aldrich) and trifluoromethane sulfonic acid (TfOH) (99%, Kanto Chem.) were used as received.

Synthesis of [dema][TfO] and Sulfonated Polyimides. [dema][TfO] was prepared by neutralization of TfOH with an equimolar amount of DEMA,[24] after which it was dried under vacuum at 80 °C for 24 h and then restored in a glovebox (VAC, $[O_2] < 1$ ppm, $[H_2O] < 1$ ppm) under an argon atmosphere. All SPIs were synthesized by polyaddition reactions of corresponding diamine monomers and NTDA, followed by chemical imidization in the presence of benzoic acid. Figure 1 shows SPIs employed as matrix polymers for [dema][TfO] in this study. SPI multiblock copolymers (*mb*-SPI 1.39 and *sb*-SPI 1.40) were synthesized by polyaddition reactions of BDSA (or BPSA) and NTDA, followed by addition of equimolar amounts of NTDA and 3BAPPS. The typical procedure is as follows: BDSA (1.00 g, 2.9 mmol), DEMA (0.73 g, 7.2 mmol), and 10 mL of *m*-cresol were added to a 100 mL three-necked flask equipped with a magnetic stirring bar. The mixture was then stirred under a nitrogen atmosphere at 100 °C until it was completely dissolved. After adding NTDA (0.778 g, 2.9 mmol) to the flask, the mixture was heated to 175 °C and then stirred for 1.5 h. Next, 3BAPPS (1.25 g, 2.9 mmol) and NTDA (0.778 g, 2.9 mmol) were added to the mixture, and it was stirred again at 175 °C for 15 h. Benzoic acid (1.77 g, 14.5 mmol) was subsequently added, and the mixture was heated to 195 °C and stirred for another 3 h. After the reaction, the mixture was cooled to 100 °C, at which point another 70 mL of *m*-cresol was added to dilute the highly viscous solution. The solution was then slowly poured into 500 mL of acetone while stirring vigorously. The resulting yellow fibrous precipitate was collected by filtration and put into another 3 L of acetone. It was vigorously stirred for 5 h to completely remove *m*-cresol. Then, the yellow fibrous precipitate was dried in a vacuum oven at 80 °C.

Fabrication of SPI/[dema][TfO] Composite Membranes. The composite membranes were fabricated according to the solution casting method. Appropriate amounts of [dema][TfO], SPI powder, and *m*-cresol were added to a sample bottle equipped with a magnetic

stirring bar. The mixture was then stirred overnight at room temperature to dissolve the solids completely, after which it was cast on a Petri dish. Evaporation of *m*-cresol at 60 °C gave uniform composite membranes. The composite membranes were peeled from the Petri dish, dried in a vacuum oven at 80 °C for 24 h, and then stored in an argon atmosphere glovebox.

Measurements. ^{1}H NMR spectra were recorded using a spectrometer (JEOL AL-400, 400 MHz) with DMSO-d_6 as a solvent and tetramethylsilane as an internal reference. Gel permeation chromatography (GPC) was carried out using an HPLC system (Shimadzu) equipped with a column (TOSOH TSKgel GMH$_{HR}$-M), which covers molecular weight range from 100 to 4 000 000. LiBr (0.01 M) mixed with dimethylformamide was used as the eluent at a flow rate of 1 mL min^{-1}. The analyte solutions were filtered through a PTFE filter (pore size 0.2 μm) before being injected into the columns. The molecular weights of the obtained polymers were calculated using a calibration curve based on polystyrene standards.

Thermal Properties. Differential scanning calorimetry (DSC) was carried out using a Seiko Instruments DSC 220C under a nitrogen atmosphere. The samples were tightly sealed in aluminum pans in a glovebox. Next, the samples were heated to 150 °C, cooled to −150 °C, and then heated again to 150 °C at a cooling and heating rate of 10 °C min^{-1}. The DSC was recorded during the reheating scans. Thermogravimetric analysis (TGA) of the composite membranes was carried out using a Seiko Instruments TG-DTA 6200C under a nitrogen atmosphere. The samples were weighed and placed in aluminum pans, after which they were heated from room temperature to 550 °C at a heating rate of 10 °C min^{-1}.

Atomic Force Microscopy (AFM) Surface Analysis. *m*-Cresol solutions of SPI and [dema][TfO] were cast directly onto a stainless-steel AFM sample holder and dried at 60 °C. The resulting membrane was washed with methanol to remove [dema][TfO] and dried again. AFM images were recorded in the tapping mode with SPA-400 (Seiko instruments Inc.) using a Si cantilever (SI-DF20S, f = 137 kHz, spring constant = 14 N m^{-1}).

Ionic Conductivities. Ionic conductivities of the composite membranes were determined by the complex impedance method in the temperature range of 40−160 °C. The composite membranes were cut into strips 6−7 mm wide and 10 mm long and then set on two platinum-wire-electrode cells separated by a distance of 4 mm and arranged in parallel on the cells. The cells were placed in a vacuum chamber, and the membrane was again dried in vacuo. The chamber was then placed in an oven and thermally equilibrated at each temperature for 1.5 h before the measurements. The measurements were performed using a potentiostat (Autolab, PGSTAT30) at frequencies ranging from 1 Hz to 1 MHz under anhydrous conditions. The ionic conductivity σ was calculated as

$$\sigma = \frac{d}{Rtw}$$

where d is the distance between the two platinum electrodes, and R, t, and w are the resistance, thickness, and width of the composite membranes, respectively.

Fabrication of Membrane Electrode Assembly (MEA) and Single Cell Test. The single cell test of the composite membrane was performed using gas diffusion electrodes (E-TEK GDE, LT-140EW; 30% Pt on Vulcan XC-72, 0.5 mg cm^{-2}, and ionomer free). The MEA was fabricated by sandwiching a composite membrane (membrane thickness ≈40 μm) between the two GDEs without hot pressing and fixing it in a single cell holder. The MEA was tested in a single cell with a serpentine-shaped gas flow field and an active area of 4 cm^2 at ambient pressure. The H_2/O_2 fuel cell polarization curves were determined at 30 °C, 120 °C, and 140 °C using an Eiwa Corp. FC test station. Anhydrous H_2 (99.99%) and O_2 (99.6%) gases were supplied to the test station at constant flow rates (H_2/O_2 = 10−30 mL min^{-1}) without any humidification.

RESULTS

Polymer Synthesis and Fabrication of Composite Membranes. Table 1 lists the molecular characterization of the synthesized SPIs. The weight-averaged molecular weights (M_w) of the SPIs were greater than 1 × 10^5 in most cases and the IECs determined by titration or ^{1}H NMR spectra agreed reasonably well with those calculated from the feed ratio of monomers, indicating that the polymerization was successful for all SPIs. The composite membranes prepared by the solution casting method were uniform, transparent, and ductile. The synthesized polymers were abbreviated as listed in Table 1, and the chemical structures are shown in Figure 1. The amount of [dema][TfO] in the composite membranes is shown in parentheses in wt% after the abbreviation of the matrix polymer (e.g., *sr*-SPI 1.88 (50)).

Table 1. Characterization of Synthesized SPIs

polymers	IEC[a] (meq g^{-1})	IEC (meq g^{-1})	M_n(× 10^5)	M_w (× 10^5)	M_w/M_n
mr-SPI 1.41	1.41	1.41[b]	2.42	5.38	2.22
mr-SPI 2.15	2.18	2.15[b]	3.79	9.42	2.48
sr-SPI 1.23	1.31	1.23[c]	1.31	2.29	1.75
sr-SPI 1.88	1.94	1.88[c]	1.05	2.49	2.37
mb-SPI 1.39	1.41	1.39[c]	2.05	4.24	2.07
sb-SPI 1.40	1.31	1.40[c]	0.78	1.86	2.39
homo-SPI 2.66	2.66	-	3.80	11.0	2.89

[a]IEC calculated from the feed monomer ratio. [b]IEC calculated from the ^{1}H NMR spectrum. [c]IEC determined by titration.

Thermal Stability. Figure 2 shows the thermogravimetric (TG) curves of the composite membranes including 50 wt % [dema][TfO]. The T_d values of all the composite membranes were greater than 250 °C and sufficient for operation of our fuel cell. The first weight loss at ca. 260 °C corresponds to elimination of the sulfonate groups in the matrix polymer, while the abrupt weight loss at 360 °C corresponds to the decomposition of [dema][TfO]. Thus, the residual weight of each composite membrane at temperatures higher than 400 °C corresponds to the polymer backbone of the matrix polymer. Figure S1 in the Supporting Information shows the TG curves of other composite membranes.

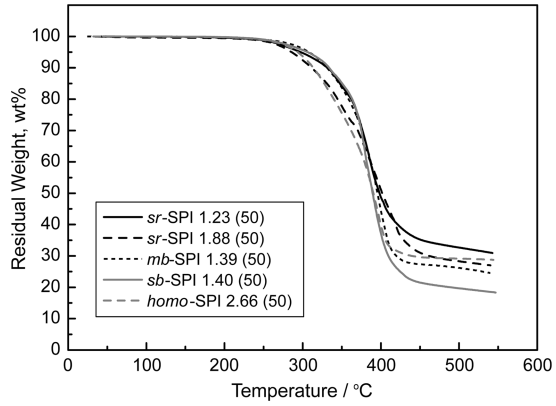

Figure 2. TG curves of the composite membrane including 50 wt % [dema][TfO].

Compatibility of [dema][TfO] in SPIs. It has previously been reported that [dema][TfO]/SPI composite membranes

show an endothermic peak corresponding to the melting point of [dema][TfO] when free [dema][TfO] remains in the membranes, and that SPIs with higher IEC values can retain higher amounts of [dema][TfO].[26] Figure 3 shows the DSC thermograms of the composite membranes based on *sr*-SPI 1.23, *sr*-SPI 1.88, and *mb*-SPI 1.39. DSC thermograms of other composite membranes are shown in Figure S2 in the Supporting Information. The presence of ammonium sulfonate groups in the polymers plays a definite role on the compatibility with [dema][TfO], as was previously reported for *mr*-SPI based composite membranes.[26] Actually, polyimides without ammonium sulfonate groups show no compatibility with [dema][TfO]. In the DSC thermograms, *sr*-SPI-1.23 (X) shows an endothermic peak at T_m of [dema][TfO] when the amounts of [dema][TfO] (X) are greater than or equal to 75% (Figure 3A). These results are similar to those obtained for *mr*-SPI 1.41 (X) (see Figure S2 in the Supporting Information), indicating that the compatibility of [dema][TfO] is similar between *sr*-SPI 1.23 and *mr*-SPI 1.41. On the other hand, no endothermic peak is observed for *mb*-SPI 1.39(X) at up to 80 wt %, despite the matrix polymer having a similar IEC value (Figure 3C). It has been reported that multiblock copolymers consisting of ionic and nonionic blocks for proton-conducting polymer electrolytes induce more developed phase separation between ionic and nonionic domains than corresponding random copolymers.[32,33] Such developed phase separation is advantageous for achieving compatibility with a large amount of [dema][TfO] via interaction with the ionic domain. Details of this phase separation are discussed in the following section.

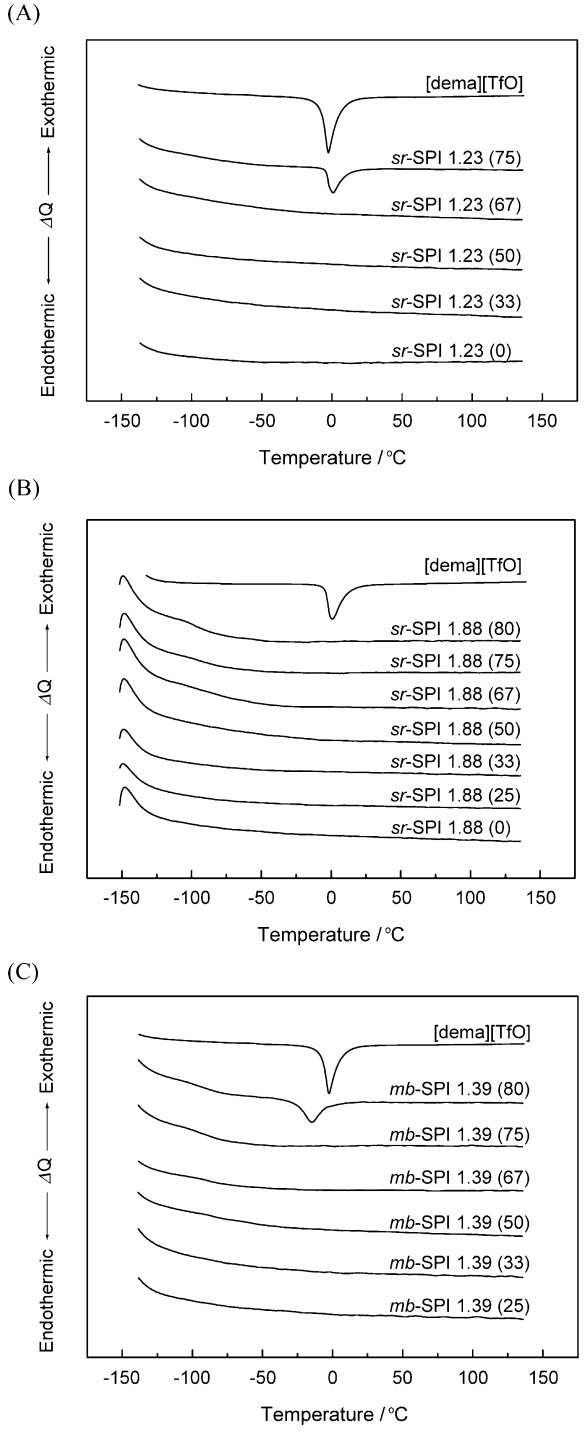

Figure 3. DSC thermograms of (a) *sr*-SPI 1.23 (X), (b) *sr*-SPI 1.88 (X), and (c) *mb*-SPI 1.39 (X).

Membrane Morphology Observed by AFM. The surface morphology of the composite membranes was observed using AMF techniques. First, we attempted to observe pristine surfaces of the composite membranes. However, clear AFM images could not be obtained owing to the highly wetted surface originating from the hygroscopic nature of [dema][TfO]. Therefore, the AFM images were recorded after removal [dema][TfO] by washing with methanol and subsequent drying under reduced pressure. Figure 4A shows the AFM phase image of *mr*-SPI 2.15 (0) and *mr*-SPI 2.15 (50). The bright region can be assigned to the soft domain, while the dark region can be assigned to the hard domain. *mr*-SPI 2.15 (0) is found to form a phase-separated structure composed of

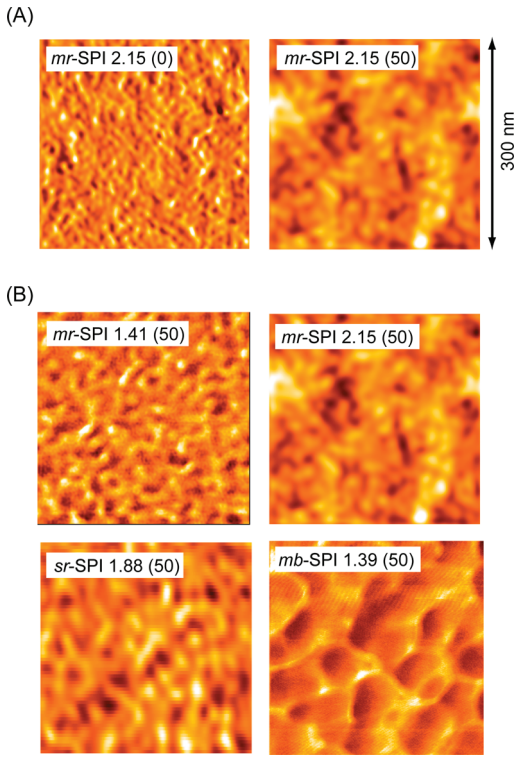

Figure 4. AFM phase images of (A) *mr*-SPI 2.15 (0) and *mr*-SPI 2.15 (50) and (B) composite membranes including 50 wt % [dema][TfO] after washing out [dema][TfO].

hard and soft domains with sizes of ca. 10 nm. On the other hand, *mr*-SPI 2.15 (50) shows a larger phase-separated structure with a domain size of ca. 15 nm, indicating that the presence of [dema][TfO] during the membrane casting facilitates the formation of larger domains. Figure 4B shows the AFM phase images of different composite membranes with 50 wt % [dema][TfO]. For all composite membranes, phase separation can be observed with different domain sizes. The domain size appears to reflect the IEC values, flexibility of the sulfonate groups (i.e., in the main chain or in the side chain), and the sequence distribution of the sulfonate groups (i.e., random or multiblock copolymers). It should be noted that *mb*-SPI 1.39 (50) shows the most developed phase separation with large domains, as seen in Figure 4B.

Ionic Conductivity. Figure 5A shows the Arrhenius plot of ionic conductivity for the *sr*-SPI 1.88 (X) composite membranes with different [dema][TfO] contents under anhydrous conditions. The ionic conductivity increases and the activation energy for conduction decreases as the [dema][TfO] content increases. The logarithmic increase in the ionic conductivity is not linear but greatly accelerates for the membranes with [dema][TfO] contents ranging from 33 to 67 wt %, as was also observed for the *mr*-SPI 1.41- and 2.15-based composite membranes.[26] These results indicate that [dema][TfO] is preferentially incorporated into the ionic domains of the phase-separated SPI to form continuous and well-developed ionic channels. When the [dema][TfO] content is small, the ionic channel has not been well developed, and the incorporated [dema][TfO] sufficiently interacts with the sulfonate groups in the polymers, resulting in large activation energies. As the [dema][TfO] contents increase, the connection of the ionic channels becomes greatly developed. Consequently, *sr*-SPI 1.88 (80) exhibited an ionic conductivity of 15.4 and 3.0 mS cm^{-1} at 160 and 40 °C, respectively.

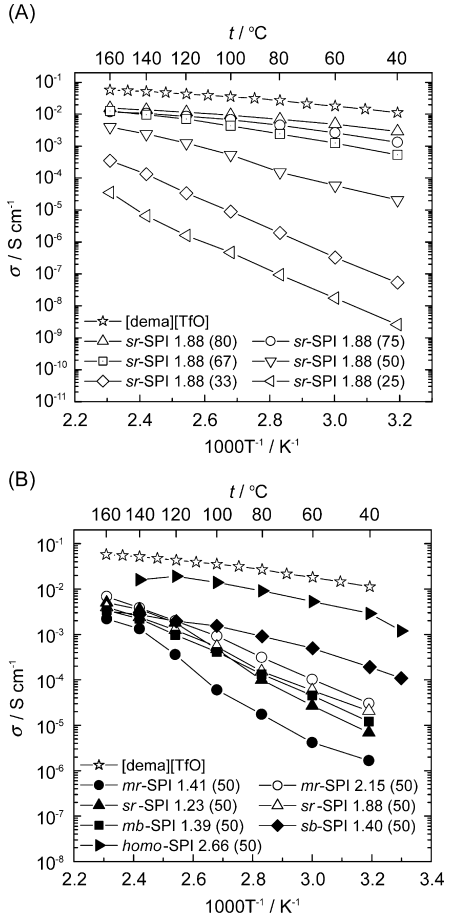

Figure 5. Arrhenius plot of ionic conductivity under anhydrous conditions. (A) *sr*-SPI 1.88 (X) and (B) composite membranes including 50 wt % [dema][TfO]. Data for *mr*-SPI 1.41 (X), *mr*-SPI 2.15 (X), and [dema][TfO] are from ref 26.

Figure 5B shows the Arrhenius plot of ionic conductivity for the composite membranes from different SPIs containing 50 wt % [dema][TfO]. At high temperatures, the difference in ionic conductivity depending on the polymer structures is small except for *homo*-SPI 2.66 (50). However, because of the difference in temperature dependence, the ionic conductivity at low temperatures differs greatly depending on the matrix polymers. Among them, *mr*-SPI 1.41 (50) exhibits the largest temperature dependency, resulting in a poor conductivity of 1.7×10^{-6} S cm^{-1} at 40 °C. On the other hand, *mr*-SPI 2.15 (50) shows relatively small temperature dependency and exhibits 3.0×10^{-5} S cm^{-1} at 40 °C. This tendency can be observed for *sr*-SPI 1.23 (50) and *sr*-SPI 1.88 (50), indicating that a high IEC of the matrix polymer is advantageous for the formation of ion conduction paths, as previously reported.[26] Comparison of the chemical structure of the matrix polymer revealed that *sr*-SPI 1.23 (50) and *mb*-SPI 1.39 (50) exhibit higher ionic conductivity than *mr*-SPI 1.41 (50), despite the similar IEC values of the matrix polymers. The sequence distribution (random or multiblock) and flexibility of sulfonate groups in the matrix polymers strongly influence the ionic conductivity. The multiblock sequence of sulfonate groups that facilitates phase separation and the flexible sulfopropoxy groups are advantageous for enhancement of the ionic conduction. Interestingly, these effects work cooperatively in *sb*-SPI 1.40 (50), which exhibits conductivity nearly 2 orders of magnitude higher (1.1×10^{-4} S cm^{-1}) than that of *mr*-SPI 1.41 (50) at 40 °C. Furthermore, *homo*-SPI 2.66 (50) exhibits the highest ionic conductivity, reaching 1.2×10^{-3} S cm^{-1} at 40 °C. A drawback of *homo*-SPI 2.66 is that it has relatively low mechanical stability, which may cause a decrease in the ionic conductivity at the highest temperature (140 °C) in Figure 5B.

Fuel Cell Performance under Nonhumidified Conditions. Figure 6 shows the polarization curves of fuel cells using the m*r*-SPI 2.15 (75) and *homo*-SPI 2.66 (80)

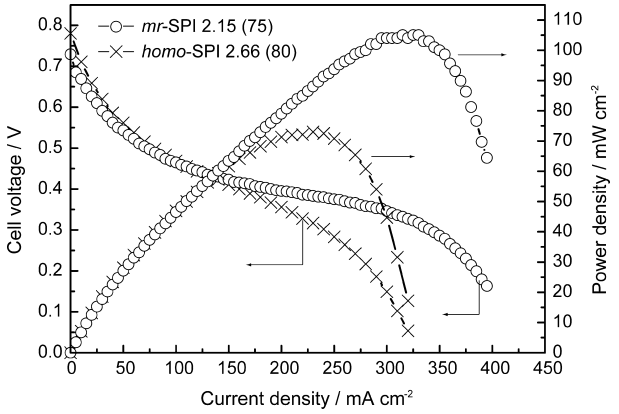

Figure 6. Polarization curves of H_2/O_2 fuel cell operation without humidification obtained using two different SPI/[dema][TfO] composite membranes at 120 °C.

dx.doi.org/10.1021/am300031k | ACS Appl. Mater. Interfaces 2012, 4, 1783−1790

membranes under nonhumidified conditions at 120 °C. In a previous study,[26] we demonstrated that a nonhumidified fuel cell using SPI/[dema][TfO] composite membranes could be operated at a maximum power density of 60 mW cm^{-2} at 120 °C. Fuel cell operation under the same conditions used in this study gave better results, with maximum power densities of 100 mW cm^{-2} for *mr*-SPI 2.15 (75) and of 70 mW cm^{-2} for *homo*-SPI 2.66 (80). Although the ionic conductivity of *homo*-SPI 2.66 (80) is higher than that of *mr*-SPI 2.15 (75), the fuel cell performance of the latter is better than the former. We assume that the three phase interfaces between gas (O_2 or H_2), proton conductor ([dema][TfO]), and Pt catalyst in the catalyst layer play a critical role in the fuel cell performance. However, we have not yet established a methodology to fabricate a proton-conducting layer on the Pt catalyst that would function even under nonhumidified conditions. The proton-conducting layer corresponds to the H^+-conducting ionomer layer in conventional humidified PEFCs prepared using perfluorinated sulfonic acid membranes. Thus, the Pt catalyst promotes fuel cell reactions only when it is in contact with [dema][TfO], which may leak slightly from the composite membranes. However, we believe that improvement of the ionic conductivity of the [dema][TfO]/SPI composite membranes is essential to achieving a high current density comparable to conventional humidified PEFCs.

DISCUSSION

Compatibility between SPI and [dema][TfO]. From a DSC thermogram of [dema][TfO], the enthalpy of fusion for [dema][TfO] was determined to be 15.5 kJ mol^{-1}. The SPI/[dema][TfO] composite membranes that include free [dema][TfO] exhibit endothermic peaks corresponding to the melting point (vide supra). Thus, the amount of [dema][TfO] that strongly interacts with the SPIs and cannot crystallize in the membranes can be estimated. The limit of the number of [dema][TfO] per ammonium sulfonate group in polymer, λ_{limit}, that strongly interact with the SPIs can be calculated from the following equation:

$$\lambda_{limit} = (N^o - N_{free})/N_{SO3H}$$

where N^o, N_{free}, and N_{SO3H} are the total amount of [dema][TfO], total amount of free [dema][TfO], and the number of ammonium sulfonate groups in the composite membranes, respectively. The results are listed in Table 2. Interestingly, the λ_{limit} value of *mr*-SPI 1.41 is 3.7, while that of *mr*-SPI 2.15 is 5.6. In other words, an increase in the limiting amount of [dema][TfO] that strongly interacts with polymer (λ_{limit}) is accelerated by an increase in the number of sulfonate groups in polymer (IEC). This phenomenon is more pronounced for *sr*-SPI based composite membranes; specifically, the λ_{limit} value of *sr*-SPI 1.23 is 4.7, whereas that of *sr*-SPI 1.88 is greater than 8.9. *mb*-SPI 1.39 shows a higher λ_{limit} than *mr*-SPI 1.41 and *sr*-SPI 1.23, even though they have similar IEC values. When a comparison is made between *mr*-SPI, *sr*-SPI, and *mb*-SPI, which have similar IECs at the same [dema][TfO] contents, the ionic domain size of *sr*-SPI and *mb*-SPI becomes larger than that of *mr*-SPI (vide supra, Figure 4). The large ionic domain in which sulfonate groups are highly aggregated is advantageous to interaction with [dema][TfO], resulting in large λ_{limit} values. The reason for the small λ_{limit} value of *homo*-SPI 2.66 at 6.1 is still not clear. To incorporate [dema][TfO] in large quantity with sufficient interaction with the sulfonate groups might require nonionic domains surrounding the ionic domains.

Table 2. Ionic Conductivity of Composite Membranes including 50 wt % [dema][TfO] at 120 °C under Anhydrous Conditions (σ_{50}) and λ Values[a]

matrix polymers	σ_{50} (mS cm^{-1})	λ[b] 33 (wt %)	50 (wt %)	67 (wt %)	λ_{limit}
mr-SPI 1.41	0.36	1.5	3.0	6.0	3.7
mr-SPI 2.15	1.99	1.0	2.0	3.9	5.6
sr-SPI 1.23	1.81	1.7	3.4	6.9	4.7
sr-SPI 1.88	1.25	1.1	2.2	4.5	>8.9[c]
mb-SPI 1.39	0.98	1.5	3.0	6.1	9.2
sb-SPI 1.40	1.95	1.5	3.0	6.0	5.6
homo-SPI 2.66	14.0	0.8	1.6	3.2	6.1

[a] λ_{limit} was determined as described in the manuscript. [b] λ = [dema][TfO]/[sulfonate group]. [c] The λ_{limit} value of *sr*-SPI 1.88 could not be determined because no obvious endothermic peak was observed, even at 80 wt %, as shown in Figure 3b.

Comparison with Hydrated Proton-Conducting Polymer Electrolytes. Kreuer et al. investigated the nature of water incorporated in proton-conducting polymer electrolyte membranes and studied the relationship between the amounts of water and the proton conductivity.[34] They reported that there are three types of water: water for primary hydration, loosely bound water, and free water. As the amount of water in the membranes increases, these three different states of water appear in this order. In the case of Nafion, a large increase in the proton conductivity is observed as the amount of loosely bound water increases (see Figure S4 in the Supporting Information). On the other hand, the proton conductivity of a hydrocarbon polymer electrolyte, sulfonated poly (ether ether ketone) (SPEEK), is greatly enhanced when the amount of free water increases. They claimed that the hydrocarbon polymer electrolyte has poor connectivity to the proton-conducting channel because of the poor phase separation. Accordingly, a larger amount of water is required for proton conduction when compared with Nafion. Figure 7 shows the relationship between λ ([dema][TfO]/[sulfonate group]) and ionic

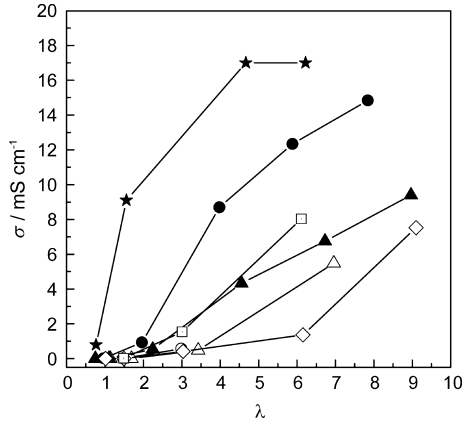

Figure 7. Relationship between λ and ionic conductivity at 120 °C. Open symbols indicate SPI-based composite membranes with low IECs, *sr*-SPI 1.23 (triangle), *mb*-SPI 1.39 (diamond), and *sb*-SPI 1.40 (square), whereas closed symbols indicate SPI-based composite membranes high IECs, *mr*-SPI 2.15 (circle), *sr*-SPI 1.88 (triangle), and *homo*-SPI 2.66 (star).

conductivity for the SPI/[dema][TfO] composite membranes. A large increase in the ionic conductivity was observed from the [dema][TfO] contents of 33−67 wt % (vide supra), which was considered to be due to development of the connectivity of ionic domains. Table 2 lists the λ values when the [dema]-[TfO] contents are 33, 50, and 67 wt % for each membrane. Comparison of the λ values with the corresponding λ_{limit} values reveals a large increase in the ionic conductivity before free [dema][TfO] appears. This phenomenon differs from that of hydrated SPEEK reported by Kreuer et al.

For hydrated proton-conducting polymer electrolytes, the number of proton carriers (i.e., hydronium cations) increases with increasing IEC values. However, the diffusivity of the proton carrier tends to be suppressed with increasing IEC values. Consequently, polymer electrolytes with higher IEC values often exhibit lower proton conductivity than those with lower IEC values when the water content is the same (especially at low water uptakes).[35] On the other hand, in the case of the SPI/[dema][TfO] composite membranes, SPI with higher IEC exhibits higher ionic conductivity if the [dema][TfO] content is the same. This result contrasts the previous results obtained for hydrated polymer electrolyte membranes.[35] Even if incorporated [dema][TfO] strongly interacts with SPI so that it cannot crystallize, a large increase in the ionic conductivity is observed. A distinct difference between the hydrated proton-conducting membranes and the SPI/[dema][TfO] composite membranes exists in that water is basically a nonionic molecular liquid, but [dema][TfO] is an ionic liquid. Thus, the atmosphere around the sulfonate groups for the SPI/[dema][TfO] is highly ionic when [dema][TfO] is incorporated into the SPIs. This highly ionic atmosphere reduces Coulombic interactions around the sulfonate groups because of the charge screening effect.[36] Further, [dema][TfO] is synthesized by neutralization between a strong Brønsted base and a superstrong Brønsted acid; therefore, the Lewis acidity of the conjugated cation and the Lewis basicity of the conjugated anion are relatively weak and have low coordination properties. The added [dema][TfO] also enhances the ionic mobility via a plasticizing effect toward the SPIs.[26] Thus, the number of ionic carriers and their mobility in the SPI/[dema][TfO] increases through an increase in the IEC values of the matrix polymer as well as in response to the amount of [dema][TfO] content. Conversely, the majority of water molecules incorporated into the polymer electrolytes exist as neutral molecules, whereas a portion of the water molecules incorporated into the polymer electrolytes form hydronium cations that can be trapped by the sulfonate anions affixed to the polymers.

CONCLUSIONS

In this study, matrix polymers with different magnitudes of IECs, different sequence distributions of ionic groups, and positions of sulfonate groups in the main chain or side chain were synthesized to investigate the effects of polymer structure on the properties of SPI/[dema][TfO] composite membranes for nonhumidified fuel cell applications. The results revealed that *mb*-SPI 1.39 (X) and *sr*-SPI 1.23 (X) exhibit higher ionic conductivity than *mr*-SPI 1.41 (X), despite having similar IEC values, indicating that the flexibility of sulfonic acid groups and the sequence distribution of ionic groups greatly affect the ion conduction. Interestingly, *homo*-SPI 2.66 (X) exhibits the highest ionic conductivity. These results strongly suggest the importance of phase separation between the ionic and nonionic domains and the connectivity of the ionic domain for achieving high ionic conductivity. A large increase in the ionic conductivity is observed as the [dema][TfO] contents increases from 33 to 67 wt %, which is likely because the incorporated [dema][TfO] strongly interacts with the sulfonate groups of SPIs to develop ionic channels.

ASSOCIATED CONTENT

Supporting Information

TG, DSC, temperature, and λ dependence of ionic conductivity. This material is available free of charge via the Internet at http://pubs.acs.org.

AUTHOR INFORMATION

Corresponding Author

*Fax: +81-45-339-3955. E-mail: mwatanab@ynu.ac.jp.

Notes

The authors declare no competing financial interest.

ACKNOWLEDGMENTS

This research was supported in part by Grants-in-Aid for Scientific Research from the MEXT of Japan (452/17073009 and A/23245046) and by a NEDO Technology Research Grant.

REFERENCES

(1) Nakagawa, H.; Izuchi, S.; Kuwana, K.; Nukuda, T.; Aihara, Y. *J. Electrochem. Soc.* **2003**, *150*, A695.
(2) Sakaebe, H.; Matsumoto, H. *Electrochem. Commun.* **2003**, *5*, 594.
(3) Ishikawa, M.; Sugimoto, T.; Kikuta, M.; Ishiko, E.; Kono, M. *J. Power Sources* **2006**, *162*, 658.
(4) Nanjundiah, C.; McDevitt, S. F.; Koch, V. R. *J. Electrochem. Soc.* **1997**, *144*, 3392.
(5) Barisci, J. N.; Wallace, G. G.; MacFarlane, D. R.; Baughman, R. H. *Electrochem. Commun.* **2004**, *6*, 22.
(6) Fukushima, T.; Asaka, K.; Kosaka, A.; Aida, T. *Angew. Chem., Int. Ed.* **2005**, *44*, 2410.
(7) Bennett, M. D.; Leo, D. J. *Sens. Actuators* **2006**, *173*, A 126.
(8) O'Regan, B.; Grätzel, M. *Nature* **1991**, *353*, 737.
(9) Papageorgiou, N.; Athanassov, Y.; Armand, M.; Bonhôte, P.; Patterson, H.; Azam, A.; Grätzel, M. *J. Electrochem. Soc.* **1996**, *143*, 3099.
(10) Kawano, R.; Watanabe, M. *Chem. Commun.* **2003**, 330.
(11) Kawano, R.; Matsui, H.; Matsuyama, C.; Sato, A.; Susan, M. A. B. H.; Tanabe, N.; Watanabe, M. *J. Photochem. Photobiol. A, Chem.* **2004**, *164*, 87.
(12) Susan, M. A. B. H.; Noda, A.; Mitsushima, S.; Watanabe, M. *Chem. Commun.* **2003**, 938.
(13) Belieres, J.-P.; Gervasio, D.; Angell, A. C. *Chem. Commun.* **2006**, 4799.
(14) Hagiwara, R.; Nohira, T.; Matsumoto, K.; Tamba, Y. *Electrochem. Solid-State Lett.* **2005**, *8*, A231.
(15) Lee, J. S.; Nohira, T.; Hagiwara, R. *J. Power Sources* **2007**, *171*, 535.
(16) Tokuda, H.; Tsuzuki, S.; Susan, M. A. B. H.; Hayamizu, K.; Watanabe, M. *J. Phys. Chem. B* **2006**, *110*, 19593.
(17) Michot, T.; Nishimoto, A.; Watanabe, M. *Electrochim. Acta* **2000**, *45*, 1347.
(18) Susan, M. A. B. H.; Kaneko, T.; Noda, A.; Watanabe, M. *J. Am. Chem. Soc.* **2005**, *127*, 4976.
(19) Ueno, K.; Hata, K; Katakabe, T.; Kondoh, M.; Watanabe, M. *J. Phys. Chem. B* **2008**, *112*, 9013.
(20) Li, Q.; He, R.; Jensen, J. O.; Bjerrum, N. *J. Chem. Mater.* **2003**, *15*, 4896.
(21) Zhang, J.; Xie, Z.; Zhang, J.; Tang, Y.; Song, C.; Navessin, T.; Shi, Z.; Song, D.; Wang, H.; Wilkinson, D. P.; Liu, Z.-S.; Holdcroft, S. *J. Power Sources* **2006**, *160*, 872.

(22) Hickner, M. A.; Ghassemi, H.; Kim, Y.-S.; Einsla, B. R.; McGrath, J. E. *Chem. Rev.* **2004**, *104*, 4587.
(23) Yang, C.; Costamagna, P.; Srinivasam, S.; Benziger, J.; Bocarsly, A. B. *J. Power Sources* **2001**, *103*, 1.
(24) Nakamoto, H.; Watanabe, M. *Chem. Commun.* **2007**, 2539.
(25) Lee, S.-Y.; Yasuda, T.; Watanabe, M. *J. Power Sources.* **2010**, *195*, 5909.
(26) Lee, S.-Y.; Ogawa, A.; Kanno, M.; Nakamoto, H.; Yasuda, T.; Watanabe, M. *J. Am. Chem. Soc.* **2010**, *132*, 9764.
(27) Yin, Y.; Suto, Y.; Sakabe, T.; Chen, S.; Hayashi, S.; Mishima, T.; Yamada, O.; Tanaka, K.; Kita, H.; Okamoto, K. *Macromolecules* **2006**, *39*, 1189.
(28) Asano, N.; Aoki, M.; Suzuki, S.; Miyatake, K.; Uchida, H.; Watanabe, M. *J. Am. Chem. Soc.* **2006**, *128*, 1762.
(29) Peckham, T. J.; Schmeisser, J.; Rodgers, M.; Holdcroft, S. *J. Mater. Chem.* **2007**, *17*, 3255.
(30) Essafi, W.; Gebel, G.; Mercier, R. *Macromolecules* **2003**, *37*, 1431.
(31) Jönsson, N. A.; Merenyi, F.; Svahn, C. M.; Gullander, J. *Acta Chem. Scand.* **1978**, *B 32*, 317.
(32) Bae, B.; Miyatake, K.; Watanabe, M. *Macromolecules* **2010**, *43*, 2684.
(33) Einsla, M. L.; Kim, Y.-S.; Hawley, M.; Lee, H.-S.; McGrath, J. E.; Liu, B.; Guiver, M. D.; Pivovar, B. S. *Chem. Mater.* **2008**, *20*, 5636.
(34) Kreuer, K. D. *Solid State Ionics* **1997**, *97*, 1.
(35) Miyatake, K.; Yasuda, T.; Watanabe, M. *J. Polym. Sci., Part A: Polym. Chem.* **2008**, *46*, 4469.
(36) Lynden-Bell, R. M. *Phys. Chem. Chem. Phys.* **2010**, *12*, 1733.